University of New Hampshire
University of New Hampshire Scholars' Repository

New Hampshire EPSCoR | Research Institutes, Centers and Programs

2-1-2022

Bimetallic Two-Dimensional Metal–Organic Frameworks for the Chemiresistive Detection of Carbon Monoxide

Aylin Aykanat
Dartmouth College

Zheng Meng
Dartmouth College

Robert M. Stolz
Dartmouth College

Colin T. Morrell
Dartmouth College

Katherine A. Mirica
Dartmouth College

Follow this and additional works at: https://scholars.unh.edu/nh_epscor

Comments

This is an Author Manuscript of an article published by Wiley in Angewandte Chemie in 2021, Version of Record available online: https://dx.doi.org/10.1002/anie.202113665

Recommended Citation

A. Aykanat, Z. Meng, R. M. Stolz, C. T. Morrell, K. A. Mirica, Angew. Chem. Int. Ed. 2022, 61, e202113665.

This Article is brought to you for free and open access by the Research Institutes, Centers and Programs at University of New Hampshire Scholars' Repository. It has been accepted for inclusion in New Hampshire EPSCoR by an authorized administrator of University of New Hampshire Scholars' Repository. For more information, please contact Scholarly.Communication@unh.edu.

Author Manuscript

Author Manuscript

Author Manuscript

Author Manuscript

HHS Public Access

Author manuscript

Angew Chem Int Ed Engl. Author manuscript; available in PMC 2023 February 01.

Published in final edited form as:

Angew Chem Int Ed Engl. 2022 February 01; 61(6): e202113665. doi:10.1002/anie.202113665.

Bimetallic Two-Dimensional Metal–Organic Frameworks for the Chemiresistive Detection of Carbon Monoxide

Aylin Aykanat[†,a], **Zheng Meng**[†,a], **Robert M. Stolz**[a], **Colin T. Morrell**[a], **Katherine A. Mirica**[a]

[a]Laboratory, Department of Chemistry, Dartmouth College, Hanover, New Hampshire 03755, United States

Abstract

This paper describes the demonstration of a series of heterobimetallic, isoreticular 2D conductive metal–organic frameworks (MOFs) with metallophthalocyanine (MPc, M=Co and Ni) units interconnected by Cu nodes towards low-power chemiresistive sensing of ppm-levels of carbon monoxide (CO). Devices achieve sub-part-per-million (ppm) limits of detection (LOD) of 0.53 ppm toward CO at low driving voltages of 0.1 V. MPc-based Cu-linked MOFs can continuously detect CO at 50 ppm, the permissible exposure limit required by Occupational Health and Safety Assessment Series, for multiple exposures and realize CO detection in air and humid environment. Diffuse reflectance infrared Fourier transform spectroscopy (DRIFTS), density functional theory (DFT) calculations, and comparison experiments suggest the contribution of Cu nodes for CO binding and the essential role of MPc units in tuning and amplifying the sensing response.

Graphical Abstract

katherine.a.mirica@dartmouth.edu .

[†]A.A. and Z.M. contributed equally to this work.

Institute and/or researcher Twitter usernames: Katherine Mirica @KMirica

Supporting information for this article is given via a link at the end of the document.

Author Manuscript Author Manuscript Author Manuscript Author Manuscript

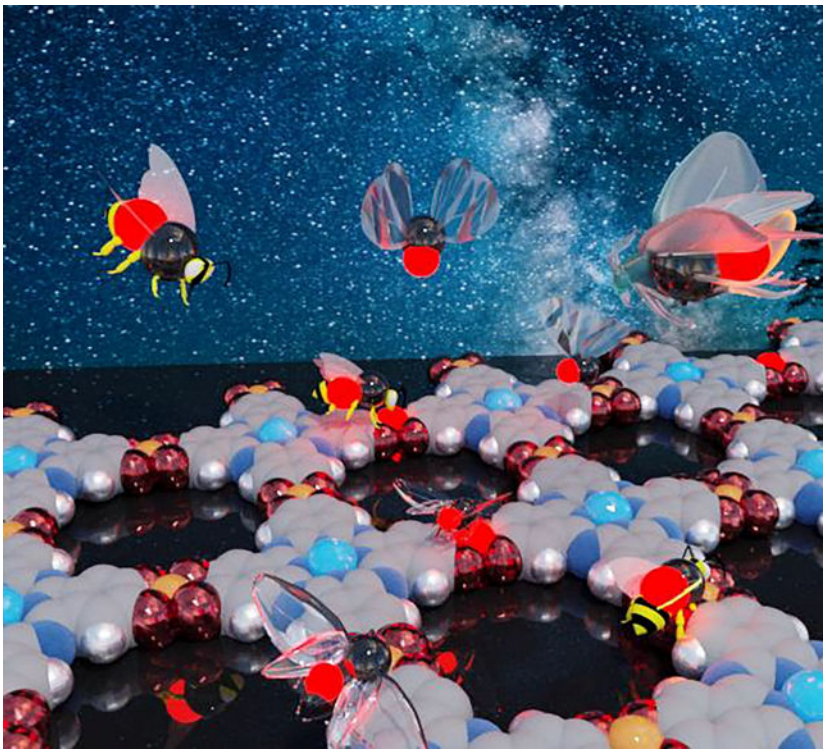

A series of isorecticular and heterobimetallic two-dimensional metal–organic frameworks achieves chemiresistive sensing of ppm concentrations of carbon monoxide at low-power. Spectroscopic techniques and computational methods, along with comparison experiments, suggest the contribution of Cu-nodes for CO binding and the essential role of metallophthalocyanine units in tuning and amplifying the sensing response.

Keywords

Metallophthalocyanine; Conductive; Two-dimensional; Metal–organic frameworks; Carbon monoxide; Chemiresistor

Introduction

The current challenges of the industrialized and fossil-powered economy demand the design and synthesis of new materials for portable sensors that detect and differentiate toxic gases, such as carbon monoxide (CO), nitrogen oxides (NO_x), and others. Among these gases, CO as a colorless, tasteless, and odorless gas is difficult to discern and responsible for more than half of all fatal poisonings worldwide.[1] Although CO detectors based on mid-infrared spectroscopy,[2] gas chromatography,[3] electrochemistry,[4] and microelectro-mechanical systems[5] are currently available, each of these systems still has limitations centered around device portability, relatively high costs, high power consumption, and low sensitivity.[6] Compared with these techniques, chemiresistive sensors that rely on the conductance change of materials upon their interaction with analytes offer the advantages of being simple, versatile, low-power, and cost-effective.[7].

Author Manuscript Author Manuscript Author Manuscript Author Manuscript

Several classes of conductive nanomaterials have been utilized for chemiresistive detection of carbon monoxide, including metal oxides,[6a, 8] carbon nanotubes (CNT),[9] and graphene.[10] However, most existing chemiresistive nanomaterials for CO sensing require high temperatures to increase sensitivity and/or post-synthetic modifications to reduce cross-sensitivity to various gaseous interferents.[6a, 9a, 11] Metal oxides, employing oxidation/reduction charge transfer reactions using surface-bound oxygen ions,[12] require high operating temperatures (>100 °C) or relatively high driving voltage (>1.5 V) to achieve sensitivity and doping with metals to improve the selectivity,[12–13] which restrict device miniaturization and mobile deployment. Single-walled carbon nanotubes modified with iron porphyrin units[14] and organometallic complexes[9d] have achieved selective chemiresistive detection of CO, however, they showed very low sensitivities (1% response to 3000 ppm of CO), likely due to secondary perturbation mechanisms that caused inefficient electronic transduction. In addition, the use of post-synthetic modifications for the enhancement of sensing responses often generates molecularly heterogeneous materials, the mechanisms of which may be challenging to elucidate.[14] Therefore, new chemiresistive materials that can meet the need for the fabrication of CO sensing devices with the features of low-power, ultra-sensitivity, and low-cost are highly desirable.[6a]

Recently, two-dimensional (2D) conductive metal–organic frameworks (MOFs) have emerged as promising materials in chemiresistive sensing.[15] This class of conductive materials possesses several advantageous characteristics for electronic chemical detection, including ease of accessibility through bottom-up synthesis,[16] modular molecular design for material–analyte interactions, low dimensionality for enhancing the sensitivity of detection, and good conductivity for low-power electronically transduced detection. 2D conductive MOFs with triphenylene-based 2D Kagome lattice structures interconnected through metal bis(dioxolene), metal bis(dithiolene), or metal bis(diimine) functionalities have realized chemiresistive detection for a series of gases, such as ammonia (NH_3), nitric oxide (NO), hydrogen sulfide (H_2S), and volatile organic compounds.[15a, 15b, 15d, 15e, 15h] Despite these successful examples of chemisistive detection over a wide range of gaseous analytes and VOCs, the demonstration of chemiresistive sensing of CO by MOF-based materials is still unprecedented. This sensing challenge originates from the low dipole moment of CO that leads to weak interactions within the host framework materials,[17] Consequently, the conductivity of the framework can be difficult to perturb by the presence of CO.

In this paper, we demonstrate MOF-based chemiresistive sensors for the detection of CO using a set of heterobimetallic 2D conductive MOFs MPc-O_8-Cu with integrated MPc (M=Co or Ni) moieties by Cu-based linkages. We realize the effective and reversible detection of CO at ppm concentrations at room temperature and low driving voltage of 0.1 V and achieve sub-part-per-million LOD (0.5–3.0 ppm). MPc-O_8-Cu MOFs can reliably detect CO at 50 ppm, the permissible exposure limit required by Occupational Health and Safety Assessment Series (OSHAS), for at least 7 consecutive exposures and maintain CO detection ability in air and in humid environment. Additionally, MPc-O_8-Cu MOF can successfully differentiate CO, NO, and NO_2 with ppm concentrations. Diffuse reflectance infrared Fourier transform spectroscopy (DRIFTS), density functional theory (DFT) calculations, and comparison experiments with MPc-$(NH)_8$-Cu and MPc-free MOFs,

Author Manuscript Author Manuscript Author Manuscript Author Manuscript

as well as monomeric MPc analogs, suggest the dominant contribution of Cu nodes for CO binding and the essential role of MPc units in amplifying the sensing response.

Results and Discussion

Our molecular design for achieving sensitive, low-power CO detection capitalizes on direct, bottom-up self-assembly between MPc ligands with embedded first-row transition metals (M= Co or Ni) and copper nodes (Figure S3 and S4). This molecular design was implemented for the following advantages. *First*, inspired by molecular design for CO detection previous examples,[9d, 14] we hypothesized that, to achieve sensitive chemiresistive detection towards CO, there is a need for both effective CO host sites with favorable binding and effective electronic perturbation caused by these binding events to transduce electronic perturbation. MPc molecules feature flexible, tunable, and π-conjugated electronic configurations[18] that can be susceptible to the change of chemical environments on and/or around MPc units. The diversity of MPcs would also provide the ability to tune the electronic interactions with the analyte through the choice of the central metals within MPc. [19] Therefore, the integration of MPc motifs into framework systems is expected to lead to highly sensitive and versatile platforms for CO detection.[20] *Second,* although utilizing MPc-based molecular materials (M= Fe, Ni, Cu, Pb, Zn, and Mn) as host sites for various analytes has been previously demonstrated,[20] these systems require high driving voltages (8–10 V)[21] or high temperatures (170 °C) due to their limited conductivity.[22] Direct integration of MPc motifs into d-π conjugated MOF systems is an established strategy for the construction of low dimensional and conductive materials to realize low-power gas detection.[15h] To enhance conductivity in these frameworks, we chose copper as the connecting metal nodes since its redox-active nature can result in a mixed valency state in the resulting frameworks and promote charge hopping.[15h, 23] In addition, Cu has also been identified as a potential host site for CO through π-backbonding,[24] which we reasoned could enable chemiresistive transduction of binding interactions with CO in a framework material. Thus, our molecular design embeds molecular recognition subunits with flexible π-configurations and Cu nodes to result in low-dimensional and bimetallic conductive framework materials with a high density of favorable host sites for sensitive and low-power chemiresistive sensing of CO.

The preparation of the MPc-O_8-Cu MOFs (M=Co or Ni) followed reported procedures (see Section 1 in SI for details). The structures of the MPc-O_8-Cu MOFs (M= Ni, Co) were confirmed by powder X-ray diffraction (pXRD) (Figure 1a). The peaks at $2\theta = 5.1°$, 10.0°, and 27.5° corresponded to the diffractions of (100), (200), and (001) planes, respectively. From the diffractions of (100) and (001), the M-to-M and π-π stacking distances were estimated to be 1.8 nm and 0.32 nm, respectively, comparable to the previously reported MPc-based 2D MOFs.[15h, 23a, 25] The structures of MPc-O_8-Cu were consistent with the eclipsed cofacial AA-stacking modes (Figure 1b). Brunauer-Emmett-Teller surface area by N_2 adsorption analysis at 77 K was found to be 411 $m^2\ g^{-1}$ for CoPc-O_8-Cu and 486 $m^2\ g^{-1}$ for NiPc-O_8-Cu. Scanning electron microscopy (SEM) images revealed nanometer-sized crystallites in both CoPc-O_8-Cu and NiPc-O_8-Cu MOFs (Figure 1c–d). High-resolution transmission electron microscopy (TEM) permitted visualization of regular lines and square meshes for CoPc-O_8-Cu and NiPc-O_8-Cu MOFs (insets in Figure 1c–d), respectively. The

Author Manuscript Author Manuscript Author Manuscript Author Manuscript

electrical conductivity of CoPc-O_8-Cu and NiPc-O_8-Cu measured at room temperature on pressed pellets using the four-point probe method (Section 8 in SI) was determined to be 3.4 × 10^{-3} and 1.0 × 10^{-3} S cm^{-1}, similar to previously reported MPc-based MOFs.[15h]

The X-ray photoelectron spectroscopy (XPS) survey spectrum of CoPc-O_8-Cu MOF revealed the presence of C, O, N, Co, and Cu (Figure S14). High-resolution scans of Co 2p region showed two peaks present at 796 eV and 781 eV, suggesting the presence of Co(II) (Figure S15d).[26] Electron paramagnetic resonance (EPR) spectra of CoPc-O_8-Cu exhibited a strong broad peak at g=2.09 and a weak peak at g=1.98, suggesting the presence of paramagnetic Co(II)/Cu(II) along with the minor presence of a ligand centered radical (Figure S15b) from the CoPc unit. The XPS survey spectrum of NiPc-O_8-Cu MOF displayed N, O, Cu, Ni, and C peaks (Figure S16). EPR of NiPc-O_8-Cu MOF showed a broad peak with g=2.01, indicating the presence of paramagnetic Cu(II) (Figure S17d).

Chemiresistive Responses of MPc-O_8-Cu MOFs to CO.

To examine the gas sensing properties of CoPc-O_8-Cu and NiPc-O_8-Cu MOFs, chemisresirtive devices were made by dropcasting 10 μL of MOF suspensions in water (1 mg/mL) onto interdigitated gold electrodes. The typical MOF film thicknesses on the electrodes measured using interferometry were 1–3 μm (Section 11 in SI). The resistance of the devices was in the range of 5–50 kΩ. The relatively low resistance of the devices, which was attributed to the good conductivity of MPc-O_8-Cu MOFs, permitted the use of a low driving voltage of 0.1 V to monitor the current change of the devices during sensing using a potentiostat.

As shown in Figures 2a, CoPc-O_8-Cu displayed a remarkable normalized sensing response ($-\Delta G/G_0$, see section 11.2 in Supporting Information) of 27.4 ± 0.8% after the exposure of 80 ppm of CO for 30 min. In comparison, NiPc-O_8-Cu demonstrated a lower average response of 18.9 ± 0.8% to the same concentration (Figure 2b). These high and positive response values, corresponding to effective electronic decrease of charge carriers within the materials upon CO exposure, indicated good sensitivity to CO. After further exposure to N_2 for 30 min, NiPc-O_8-Cu and CoPc-O_8-Cu demonstrated partial recovery of 68% and 67%, respectively. At the lower concentrations, the responses of the CoPc-O_8-Cu tended to be more reversible. To investigate the kinetics of sensor response, we estimated the rate constant (k) from the response plot of MPc-O_8-Cu MOFs to 20 ppm of CO according to a first-order reaction kinetic model (see section 11.2 in Supporting Information for details).[21a] The deduced rate constant between CO and CoPc-O_8-Cu was 5.0×10^{-3} s^{-1}, in comparison to 2.1×10^{-3} s^{-1} for rate constant between CO and CoPc-O_8-Cu. These rate constants are in a similar range as those found in MPc based thin film devices (k=0.15 to 0.60 min^{-1}).[21a, 27]

Plotting responses at 30 min exposure against the concentrations of CO (Figure 2c) yielded good linear relationships (R^2= 0.99) for both MPc-O_8-Cu MOFs.[21a] The LOD values were derived from the linear relationships between the response and concentration.[15d, 15h] The LOD value for CO achieved by using CoPc-O_8-Cu and NiPc-O_8-Cu were 0.53 ppm and 3.0 ppm for CO, respectively. These values are significantly below OHSAS required permissible exposure limit (50 ppm) for a time-weighted average of 8 hours for CO.[28] The LOD

Author Manuscript Author Manuscript Author Manuscript Author Manuscript

for CO obtained by CoPc-O_8-Cu at room temperature was also significantly lower than functionalized carbon nanotubes,[9d, 29] metal oxides,[30] and metal nanocomposites (Table S3).[31] We hypothesize that the high density of favorable host sites within MPc-O_8-Cu frameworks, in combination with efficient perturbation of the charge transport pathway in a low dimensional material, is responsible for the high sensitivity to CO at low concentrations. The different LODs for CO obtained by CoPc-O_8-Cu and NiPc-O_8-Cu suggested the important role of the MPc in the modulation of sensing of CO, where distinct electronic properties of the two MPc components may contribute to the affinity of the host site and the feasibility of electronic perturbation of the frameworks.

Encouraged by the reversibility of response of these MOFs to CO, we tested the capability of the MOFs to respond to consecutive exposures of CO under different concentrations. With the sequential exposure of 50 ppm of CO, both NiPc-O_8-Cu and CoPc-O_8-Cu exhibited excellent reversibility (Figure 3a), which indicated the potential of both MOFs for real-time monitoring of CO. NiPc-O_8-Cu and CoPc-O_8-Cu were able to continuously detect OHSAS required permissible exposure limits of CO at 50 ppm with high responses of 17.9 ± 0.4% and 4.4 ± 0.3%, respectively. The responses persisted for at least 7 exposures without significant loss of signal. To evaluate the CO sensing ability under conditions closer to the real-world scenario, the sensing response to CO was assessed in air and humidity (5000 ppm in N_2, 18% relative humidity, RH). Compared to the 27.4 ± 0.8% and 18.9 4 ± 0.8% responses under N_2, NiPc-O_8-Cu and CoPc-O_8-Cu still displayed high responses of 19.8 ± 0.1% and 12.3 ± 2.5% to 80 ppm of CO in air. In humid N_2, the responses of NiPc-O_8-Cu and CoPc-O_8-Cu to 80 ppm were reduced to approximately 3.1 ± 1.2% and 1.4 ± 0.1%. The diminished response observed under air and humidity, especially the latter, suggested the competitive effect from the interfering species, such as O_2 or H_2O molecules, which may partially occupy the CO binding sites in the MOFs. Despite these detrimental factors, it is worth noting that the robust responses realized by both NiPc-O_8-Cu and CoPc-O_8-Cu were still much higher than the benchmark materials of modified carbon nanotubes operating under similar conditions.[9d, 14]

Considering the superior sensing performance of CoPc-O_8-Cu over NiPc-O_8-Cu in the above tests, we further chose CoPc-O_8-Cu for the examination of its dynamic and continuous CO sensing properties in humid air. We found that, in the air with 5000 ppm of H_2O (18% relative humidity, RH), CoPc-O_8-Cu was still capable to continuously detect CO in the concentration range of 10–80 ppm for multiple exposures (Figure 3c). Moreover, plotting the sensing response versus concentration yielded excellent linearity (Figure 3d). The LOD for CO derived from the response-concentration relationship in these consecutive exposures reached 0.78 ppm by CoPc-O_8-Cu, which was only slightly higher than that obtained by 30 min CO exposure in the N_2.

The possible atmospheric interferent CO_2 only gave very low normalized responses of 0.4% and 3.1% by CoPc-O_8-Cu and NiPc-O_8-Cu at 80 ppm of CO_2, respectively (Figure 3e). In comparison to the positive response to CO, both CoPc-O_8-Cu and NiPc-O_8-Cu showed negative responses to NO_x, including NO and NO_2, which resulted in conductivity increases of the MPc-O_8-Cu MOFs (Figure 3f). Taking advantage of this distinct response characteristic to these gases, we treated the sensing data of the three gases CO, NO, and NO_2

Author Manuscript Author Manuscript Author Manuscript Author Manuscript

from the MPc-O_8-Cu MOFs by principal component analysis (PCA). As shown in Figure 4c, PCA analysis yielded clear groupings of the three gases, as indicated by the colored ovals superimposed onto the data, which demonstrated that both CoPc-O_8-Cu and NiPc-O_8-Cu MOFs were able to differentiate 80 ppm of CO, NO, and NO_2.

The two types of metal centers and coordination environments present in the MPc-O_8-Cu MOFs, MPc units and Cu bis(dioxlene) nodes, both can potentially serve as effective binding sites for the CO interaction. To identify the favorable CO interaction sites on MPc-O_8-Cu MOFs, we performed diffuse reflectance infrared Fourier transform spectroscopy (DRIFTS). DRIFTS enables IR spectra to be obtained for bulk microcrystalline samples during the in-situ exposure to the target analyte, which has been used to probe host–guest interactions between analytes and framework materials through the intensity changes or position shifts of characteristic absorption bands.[32] Upon the exposure to gas-phase CO, the spectra for both NiPc-O_8-Cu and CoPc-O_8-Cu exhibited strong and broad absorbance bands at 2090 and 2100 cm^{-1}, where the branch at 2090 cm^{-1} was more intesnse than the band at 2100 cm^{-1}. These bands corresponded to the P-branch and R-branch of gas-phase CO, respectively.[32b] With the exposure switching from CO to N_2, the P- and R-branch of gas-phase CO were readily removed, while a small positive absorbance band at 2117 cm^{-1} remained for both CoPc-O_8-Cu and NiPc-O_8-Cu (Figure 4a, 4b). In addition to the absorbance band at 2117 cm^{-1}, CoPc-O_8-Cu exhibited a set of weak and negative-going bands at 1451, 1360, and 1270 cm^{-1}. These negative-going bands observed as a result of the interaction between CO and CoPc-O_8-Cu were likely attributed to the distortion of the Cu-bis(dioxolene) units.[32a] With prolonged N_2 purging (>15 min), the band at 2117 cm^{-1} was finally removed and the negative-going bands observed in the spectra of CoPc-O_8-Cu remained. Typically, the backdonation of charge into the antibonding $2\pi^*$ orbital weakens the CO stretching frequency, which presents stretching frequencies of CO typically at 2070–2100 cm^{-1} when adsorbed on metallic copper,[33] 2120–2160 cm^{-1} when adsorbed on Cu(I)-containing zeolites,[34] and ~2170 cm^{-1} when adsorbed on Co(II) containing complexes.[35] Coupled with these typical stretching frequencies of CO adsorbed on metals with the observed CO stretching frequencies and the bands attributed to the distortion of Cu-bis(dioxolene) units, we attributed the weak band observed at 2117 cm^{-1} to the absorbance of CO on Cu Lewis acid sites (LAS) on the MPc-O_8-Cu MOFs. The small shifts of CO vibrational mode indicated that the interaction with the LAS may be weak, which was corroborated by the reversible nature of the interaction with extended purging with N_2. To provide further evidence for our assertion that the Cu center was the primary host site for adsorption of CO to the frameworks, we conducted DRIFTS experiments using molecular analogs of the phthalocyanine sites within the framework to determine their ability to adsorb CO. Among MPcs examined (where M = Mn, Fe, Co, Ni, Cu, and Zn), only the FePc analog exhibited an observable ability to adsorb CO (Figure S35). The lack of observed adsorption of CO by CoPc and NiPc was consistent with the identification of the Cu-bis(dioxolene) units as the primary host sites in CO sensing.

To gain further insight into the relatively high sensing response of the MPc-O_8-Cu MOFs and their MPc-dependent sensing response, we evaluated the interaction between CO and the MOFs and the electronic effect of the MPc-O_8-Cu MOFs perturbed by CO binding using density functional theory (DFT) calculations (See Section 12 in SI). The

Author Manuscript Author Manuscript Author Manuscript Author Manuscript

structures of CO adsorbed on the Co/Ni and Cu sites of MOFs were optimized by using the single-layer model of the MOFs in Dmol^3 module of *Materials Studio 2019*. The generalized gradient approximation with Perdew-Becke-Ernzerhof was used for the exchange-correlation function[36] with double numerical with polarization functions (DNP) as basis set, and an accurate DFT semi-core pseudopotentials was employed for the metal atoms (see section 13 in Supporting Information for details).[37] In the optimized CO-bound CoPc-O_8-Cu structure, CO molecule bound to Co and Cu atoms with metal to CO distances of 1.802 and 1.865 Å, respectively (See Section 12), which are in a similar range with other Co–CO and Cu–CO distances identified in some crystals structures of MOFs.[38] These bond length values, together with the nearly linear coordination geometry formed between CO and Co/Cu, suggested the presence of a σ-coordination bond formed between the 5σ orbital of CO and d_z^2 orbital of the metal ions, in conjunction with the contribution of π backbonding due to the overlap of the $2\pi^*$ orbitals of CO and d_{xz} or d_{yz} orbitals of the metal ions.[39] In CO-bound NiPc-O_8-Cu structure (Figure 4d), the binding of CO with Cu was similar to that for CoPc-O_8-Cu. However, the distance between Ni and CO was found significantly longer than those between CO and Co/Cu ions. The estimated free energies for CO binding at Co and Cu sites in CoPc-O_8-Cu were −6.5 and −2.9 kJ mol^{-1}; in comparison, the free energies for CO binding at Ni and Cu sites in NiPc-O_8-Cu were 16.0 and −6.8 kJ mol^{-1} (Figure 4e). These values suggested that the CO binding at the Co and Cu centers are favorable while binding at Ni is not. In the CO-bound MOF structures, CO binding to Cu cites caused noticeable distortions of the Cu-bis(dioxolene) fragment (Figure 4c, 4d), which was consistent with the results as suggested by DRIFTS. Such structural distortions can generate interfacial stress to give prominent electronic change of the sensing materials.[40] Mulliken population analysis indicated that CO binding at Co and Cu in CoPc-O_8-Cu caused the decrease of charges on Co and Cu by 0.217 and 0.179, respectively; meanwhile, the net charges of CO molecules increased (Figure 4c). These results indicated that the interaction between CO and CoPc-O_8-Cu induced a prominent CO-to-MOF charge transfer. Similar charge transfer was also found for computational assessment of CO binding at Cu in NiPc-O_8-Cu. However, the charge transfer effect may be weak upon the interaction of CO at Ni site of NiPc-O_8-Cu, as no significant change of atomic charges was associated (Figure 4c). Therefore, computational study suggested that CO binding at both Co and Cu sites of CoPc-O_8-Cu can cause an effective charge transfer effect, while CO binding at only Cu sites of NiPc-O_8-Cu can cause such effect. This difference may explain the higher magnitude of response and faster response kinetics observed for CoPc-O_8-Cu than for NiPc-O_8-Cu.[18]

The computational analysis is based on the interaction between CO and the 2D single-layer of the two MPc-O_8-Cu MOFs with theoretically prefect structure. However, it should be noted that, in addition to differences in chemical compositions, the actual mechanism responsible for the observed CO sensing response can be complicated by the contributions from crystallinity, morphology, and activation procedure of the materials, as well as by the steps of device preparation. As shown in Figure 1, the full width at half maximum (FWHM) of diffraction peaks of the CoPc-O_8-Cu are larger than that of the NiPc-O8-Cu, suggesting a lesser crystallinity for the former. According to the Scherrer equation,[38] the mean crystal sizes of CoPc-O_8-Cu and NiPc-O_8-Cu are about 90 nm and 140 nm, respectively, as estimated from the FWHM of the (100) and (200) peaks. The smaller crystallites of

Author Manuscript Author Manuscript Author Manuscript Author Manuscript

CoPc-O_8-Cu suggested the possibility of more defective sites and edge functional groups exposed in CoPc-O_8-Cu than in NiPc-O_8-Cu. In addition, the morphology of the materials as synthesized (Figure 1c and 1d) and as being deposited on the device (Figure S23) also exhibited visible differences. As all these factors can affect the availability of effective CO binding sites in the sensing materials, and consequently, the sensitivity of the materials, the precise comparison of the relative percentage of metal centers that can be viable to interact with CO was not possible.

As DRIFTS and DFT studies both pointed to the significant contributions of the Cu metal node during CO binding in MPc-O_8-Cu MOFs, we sought to identify the role of MPc units through the use of $M_3(HHTP)_2$ (HHTP=2,3,6,7,10,11-hexahydroxytriphenylene, M=Co, Ni, and Cu) MOFs that contained only metal bis(dioxolene) fragments. With 30 min exposure to CO, $Cu_3(HHTP)_2$ exhibited a response of 5.1 ± 0.8% after, which is higher than the Co and Ni analogs (2.0 ± 0.4% and 4.5 ± 0.5%, respectively), again confirming the superior contribution of the Cu node. However, we found that under the same conditions MPc-O_8-Cu MOFs showed more than 3 times higher sensing responses than the $M_3(HHTP)_2$ MOFs (Figure 4f), which evidenced the essential role of MPc units in providing strong sensing response. The above results also supported the molecular design concept by interconnecting MPc units with Cu nodes may be generally effective for realizing sensitive CO sensing. To further examine this concept, we tested the CO sensing response of two previously reported isorecticular MOFs MPc-$(NH)_8$-Cu that featured MPc ligands linked with copper nodes by NH heteroatoms (see in Supporting Information).[25b] We observed similar magnitudes of response to CO at the concentrations of 10–80 ppm in MPc-$(NH)_8$-Cu MOFs as those in MPc-O_8-Cu MOFs, confirming the key role of the MPc units in tuning the sensitivity of the Cu-nodes to CO (Figure S28).

Conclusion

In summary, we fabricated 2D MPc-O_8-Cu MOF-based chemiresistors capable of realizing low-power and sensitive detection of carbon monoxide at room temperature. This report is the first demonstration of carbon monoxide sensing using MOF-based chemiresistors. Devices made of MPc-O_8-Cu MOF achieved sub-part-per-million (ppm) detection limits toward CO (0.53–3.0 ppm) at room temperature with good reversibility and repeated detection of CO at permissible exposure limits set by OSHAS, while maintaining sensing performance in air and humid environment. MPc-O_8-Cu MOFs successfully differentiated CO, NO, and NO_2 at ppm concentrations. The sensitivity of MPc-O_8-Cu-based frameworks reported herein surpassed reported functionalized SWCNT,[9d] metal oxide sensors[12, 30b], and rival that of conductive polymers (Table S3),[41] and recently reported colorimetric sensors.[42] DRIFTS suggested that Cu nodes play a primary role in CO binding, while the identity of the metal within the MPc unit further tuned the sensitivity. DFT calculations and comparison experiments with MPc-free MOFs supported the essential role of MPc units in tuning and amplifying the sensing response, when coupled with Cu-nodes of the MOFs.

The superior sensitivity of CO detection accomplished at low driving voltage of 0.1 V and room temperature provides a practical foundation for the development of low-power toxic gas sensors. The ability to differentiate between NO and CO—a challenging limitation for

Author Manuscript Author Manuscript Author Manuscript Author Manuscript

other materials, such as metal oxides—offers an additional advantage when coupled with real-time analysis. These materials offer modular design strategies for sensitive and selective chemiresistive devices that operate over a broad dynamic range of concentrations.

It is important to note that this work achieves sensing of CO using bulk polycrystalline MOF materials and that differences in both MPc-frameworks crystallinity, morphology and defect sites can influence the sensitivity of both materials towards CO. These parameters can complicate the elucidation of binding sites and sensing mechanisms within MPc-O_8-Cu systems. Future studies focused on operando spectroscopy and other in situ analysis techniques, coupled with thin film and single crystal studies, can help overcome these limitations and provide precise insight into the role of the MPc units, Cu-nodes, and defect sites in the sensing mechanism.

Supplementary Material

Refer to Web version on PubMed Central for supplementary material.

Acknowledgements

We acknowledge support from startup funds provided by Dartmouth College, NSF CAREER Award (#1945218), Army Research Office Young Investigator Program Grant No. W911NF-17-1-0398, National Science Foundation EPSCoR award (#1757371), Cottrell Scholar Award from Research Corporation for Science Advancement (#26019), US Army Cold Regions Research and Engineering Lab (Award No. W913E519C0008), Camille Dreyfus Teacher-Scholar Award, and the Maximizing Investigators' Research Award from the National Institutes of Health (R35GM138318). The authors thank the University Instrumentation Center at the University of New Hampshire (Durham, NH) for the access of XPS.

References

[1]. Chiew AL, Buckley NA, Critical Care 2014, 18, 221.

[2] a. Dong M, Zheng C, Miao S, Song F, Wang Y, Infrared. Phys. Technol. 2017, 85, 450–456;bPal S, Ozanyan KB, McCann H, J. Phys. Conf. Ser. 2007, 85;cWerle P, Slemr F, Maurer K, Kormann R, Mücke R, Jänker B, Optics and Lasers in Engineering 2002, 37, 101–114.

[3] a. Porter K, Volman DH, Anal. Chem. 2002, 34, 748–749;bKamiński M, Kartanowicz R, Jastrzębski D, Kamiński MM, J. Chromatogr. A 2003, 989, 277–283. [PubMed: 12650260]

[4]. Guth U, Vonau W, Zosel J, Measurement Science and Technology 2009, 20, 042002.

[5]. Mujahid A, Dickert FL, Sensors 2017, 17, 2716.

[6] a. Wilson DM, Hoyt S, Janata J, Booksh K, Obando L, IEEE Sensors Journal 2001, 1, 256–274;bStetter JR, Li J, Chemical Reviews 2008, 108, 352–366. [PubMed: 18201108]

[7]. Franke ME, Koplin TJ, Simon U, Small 2006, 2, 36–50. [PubMed: 17193551]

[8]. Wetchakun K, Samerjai T, Tamaekong N, Liewhiran C, Siriwong C, Kruefu V, Wisitsoraat A, Tuantranont A, Phanichphant S, Sensors and Actuators B: Chemical 2011, 160, 580–591.

[9] a. Kauffman DR, Star A, Angew Chem Int Ed Engl 2008, 47, 6550–6570; [PubMed: 18642264] bChoi HH, Lee J, Dong K-Y, Ju B-K, Lee W, Macromolecular Research 2012, 20, 143–146;cZaporotskova IV, Boroznina NP, Parkhomenko YN, Kozhitov LV, Modern Electronic Materials 2016, 2, 95–105;dSavagatrup S, Schroeder V, He X, Lin S, He M, Yassine O, Salama KN, Zhang XX, Swager TM, Angew Chem Int Ed Engl 2017, 56, 14066–14070. [PubMed: 28952172]

[10] a. Yavari F, Koratkar N, The Journal of Physical Chemistry Letters 2012, 3, 1746–1753; [PubMed: 26291854] bSchedin F, Geim AK, Morozov SV, Hill EW, Blake P, Katsnelson MI, Novoselov KS, Nature Materials 2007, 6, 652–655; [PubMed: 17660825] cPanda D, Nandi A, Datta SK, Saha H, Majumdar S, RSC Advances 2016, 6, 47337–47348.

Author Manuscript Author Manuscript Author Manuscript Author Manuscript

[11]. Wiegleb G, Heitbaum J, Sensors and Actuators B: Chemical 1994, 17, 93–99.

[12]. Wang C, Yin L, Zhang L, Xiang D, Gao R, Sensors (Basel) 2010, 10, 2088–2106. [PubMed: 22294916]

[13] a. Wang K, Zhao T, Lian G, Yu Q, Luan C, Wang Q, Cui D, Sensors and Actuators B: Chemical 2013, 184, 33–39;bWang S, Zhao Y, Huang J, Wang Y, Kong F, Wu S, Zhang S, Huang W, Vacuum 2006, 81, 394–397.

[14]. Liu SF, Lin S, Swager TM, ACS Sens 2016, 1, 354–357. [PubMed: 27280172]

[15] a. Campbell MG, Liu SF, Swager TM, Dincă M, J. Am. Chem. Soc. 2015, 137, 13780–13783; [PubMed: 26456526] bCampbell MG, Sheberla D, Liu SF, Swager TM, Dincă M, Angew. Chem. Int. Ed. 2015, 54, 4349–4352;cSmith MK, Jensen KE, Pivak PA, Mirica KA, Chem. Mater. 2016, 28, 5264–5268;dKo M, Aykanat A, Smith MK, Mirica KA, Sensors (Basel) 2017, 17, 2192;eSmith MK, Mirica KA, J. Am. Chem. Soc. 2017, 139, 16759–16767; [PubMed: 29087700] fYao MS, Lv XJ, Fu ZH, Li WH, Deng WH, Wu GD, Xu G, Angew. Chem. Int. Ed. 2017, 56, 16510–16514;gRubio-Gimenez V, Almora-Barrios N, Escorcia-Ariza G, Galbiati M, Sessolo M, Tatay S, Marti-Gastaldo C, Angew. Chem. Int. Ed. 2018, 57, 15086–15090;hMeng Z, Aykanat A, Mirica KA, J. Am. Chem. Soc. 2019, 141, 2046–2053. [PubMed: 30596491]

[16]. Hmadeh M, Lu Z, Liu Z, Gándara F, Furukawa H, Wan S, Augustyn V, Chang R, Liao L, Zhou F, Perre E, Ozolins V, Suenaga K, Duan X, Dunn B, Yamamto Y, Terasaki O, Yaghi OM, Chemistry of Materials 2012, 24, 3511–3513.

[17] a. Karra JR, Walton KS, J. Phys. Chem. C 2010, 114, 15735–15740;bValenzano L, Civalleri B, Chavan S, Palomino GT, Areán CO, Bordiga S, J. Phys. Chem. C 2010, 114, 11185–11191;cMartín-Calvo A, Lahoz-Martín FD, Calero S, J. Phys. Chem. C 2012, 116, 6655–6663;dKim H, Sohail M, Yim K, Park YC, Chun DH, Kim HJ, Han SO, Moon JH, ACS Appl. Mater. Interfaces 2019, 11, 7014–7021; [PubMed: 30667210] eLanderos-Rivera B, Ibarra IA, Diaz-Ramirez ML, Vargas R, Lara-Garcia HA, Garza J, Martinez A, Phys. Chem. Chem. Phys. 2020, 22, 7969–7974. [PubMed: 32236261]

[18]. Aykanat A, Meng Z, Benedetto G, Mirica KA, Chemistry of Materials 2020, 32, 5372–5409.

[19]. Gould RD, Coord. Chem. Rev 1996, 156, 237–274.

[20](a). Linkous CA, O'Grady WE, Sayers D, Yang CY, Inorg. Chem. 1986, 25, 3761–3765;bStrozecka A, Soriano M, Pascual JI, Palacios JJ, Phys. Rev. Lett. 2012, 109, 147202; [PubMed: 23083274] cMukherjee D, Manjunatha R, Sampath S, Ray AK, in Materials for Chemical Sensing, Springer, 2017, pp. 165–226.

[21] a. Bohrer FI, Sharoni A, Colesniuc C, Park J, Schuller IK, Kummel AC, Trogler WC, J. Am. Chem. Soc. 2007, 129, 5640–5646; [PubMed: 17411043] bBohrer FI, Colesniuc CN, Park J, Schuller IK, Kummel AC, Trogler WC, J. Am. Chem. Soc. 2008, 130, 3712–3713. [PubMed: 18321103]

[22]. Jones TA, Bott B, Sens. and Act. 1986, 9, 27–37.

[23] a. Nagatomi H, Yanai N, Yamada T, Shiraishi K, Kimizuka N, Chem. Eur. J 2018, 24, 1806–1810; [PubMed: 29291261] bQiu XF, Zhu HL, Huang JR, Liao PQ, Chen XM, J. Am. Chem. Soc. 2021, 143, 7242–7246; [PubMed: 33956435] cMeng Z, Luo J, Li W, Mirica KA, Journal of the American Chemical Society 2020, 142, 21656–21669. [PubMed: 33305565]

[24] a. Su GM, Wang H, Barnett BR, Long JR, Prendergast D, Drisdell WS, Chem. Sci. 2021, 12, 2156–2164;bFry HC, Scaltrito DV, Karlin KD, Meyer GJ, J. Am. Chem. Soc. 2003, 125, 11866–11871; [PubMed: 14505408] cYou W, Liu Y, Howe JD, Sholl DS, J. Phys. Chem. C 2018, 122, 8960–8966.

[25] a. Chen J, Chen Z, Boussaid F, Zhang D, Pan X, Zhao H, Bermak A, Tsui C-Y, Wang X, Fan Z, ACS Nano 2018, 12, 6079–6088; [PubMed: 29792677] bMeng Z, Luo J, Li W, Mirica KA, J. Am. Chem. Soc. 2020, 142, 21656–21669. [PubMed: 33305565]

[26]. Chuang TJ, Brundle CR, Rice DW, Surf. Sci. 1976, 59, 413–429.

[27]. Tongpool R, Yoriya S, Thin Solid Films 2005, 477, 148–152.

[28]. O. S. a. H. A. (OSHA), 2017.

[29]. Liu SF, Lin S, Swager TM, ACS Sens. 2016, 1, 354–357. [PubMed: 27280172]

[30] a. Mahajan S, Jagtap S, Appl. Mater. Today 2020, 18, 100483;bAroutiounian V, Int. J. Hydrog. Energy 2007, 32, 1145–1158;cNandy T, Coutu RA Jr., Ababei C, Sensors 2018, 18.

Author Manuscript Author Manuscript Author Manuscript Author Manuscript

[31]. Ma J, Ren Y, Zhou X, Liu L, Zhu Y, Cheng X, Xu P, Li X, Deng Y, Zhao D, Advanced Functional Materials 2018, 28, 1705268.

[32] a. Stolz RM, Mahdavi-Shakib A, Frederick BG, Mirica KA, Chem. Mater. 2020, 32, 7639–7652;bHadjiivanov KI, Panayotov DA, Mihaylov MY, Ivanova EZ, Chakarova KK, Andonova SM, Drenchev NL, Chem. Rev. 2021, 121, 1286–1424. [PubMed: 33315388]

[33]. Hollins P, Pritchard J, Surface Science 1979, 89, 486–495.

[34]. Cox DF, Schulz KH, Surface Science 1991, 249, 138–148.

[35]. Bloch ED, Hudson MR, Mason JA, Chavan S, Crocellà V, Howe JD, Lee K, Dzubak AL, Queen WL, Zadrozny JM, Geier SJ, Lin L-C, Gagliardi L, Smit B, Neaton JB, Bordiga S, Brown CM, Long JR, Journal of the American Chemical Society 2014, 136, 10752–10761. [PubMed: 24999916]

[36]. Hammer B, Hansen LB, Nørskov JK, Phys. Rev. B 1999, 59, 7413–7421.

[37]. Delley B, Phys. Rev. B 2002, 66.

[38]. Gallagher AT, Malliakas CD, Harris TD, Inorg. Chem. 2017, 56, 4655–4662. [PubMed: 28379000]

[39] a. Goldman AS, Krogh-Jespersen K, J. Am. Chem. Soc. 1996, 118, 12159–12166;bLupinetti AJ, Fau S, Frenking G, Strauss SH, J. Phys. Chem. A 1997, 101, 9551–9559.

[40] a. Allendorf MD, Houk RJ, Andruszkiewicz L, Talin AA, Pikarsky J, Choudhury A, Gall KA, Hesketh PJ, J Am Chem Soc 2008, 130, 14404–14405; [PubMed: 18841964] bKamencek T, Zojer E, The Journal of Physical Chemistry C 2021.

[41]. Lin C, Xian X, Qin X, Wang D, Tsow F, Forzani E, Tao N, ACS Sensors 2018, 3, 327–333. [PubMed: 29299924]

[42]. Misra SCK, Mathur P, Srivastava BK, Sensors and Actuators A: Physical 2004, 114, 30–35.

Author Manuscript Author Manuscript Author Manuscript Author Manuscript

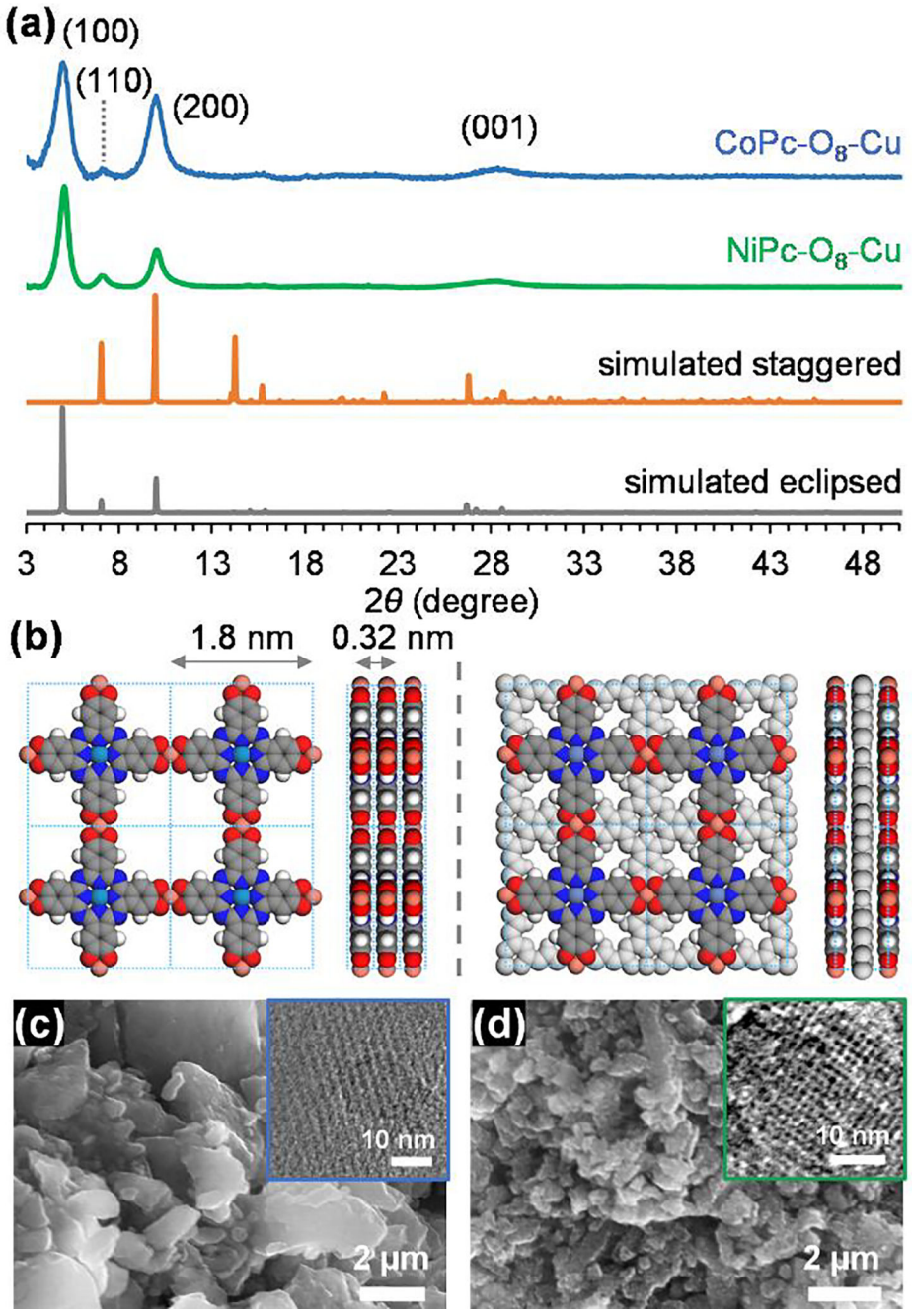

Figure 1.

(a) Experimental pXRD diffraction patterns of CoPc-O_8-Cu (blue) and NiPc-O_8-Cu (green) MOFs and simulated pXRD of MPc-O_8-Cu MOFs with eclipsed (orange) and staggered (grey) stacking. (b) Structure models of MPc-O_8-Cu MOFs with eclipsed (left) and staggered (right) stacking. SEM of images of (c) CoPc-O_8-Cu and (d) NiPc-O_8-Cu. Insets, TEM images.

Author Manuscript Author Manuscript Author Manuscript Author Manuscript

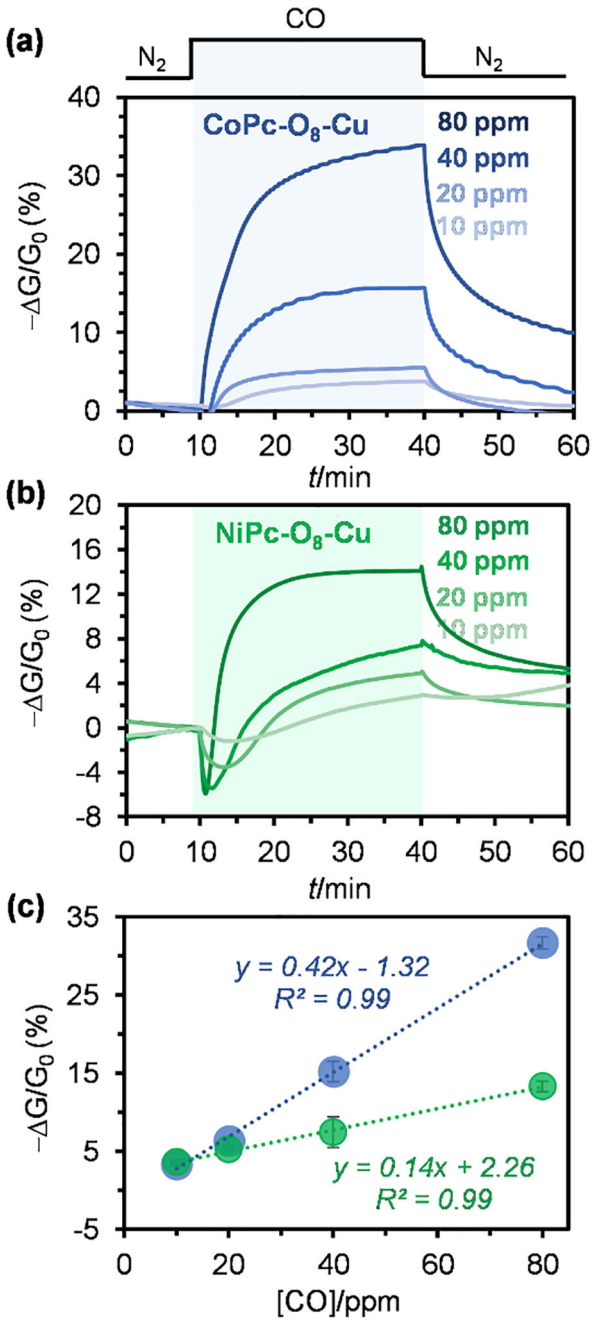

Figure 2.

Saturation sensing traces of **(a)** CoPc-O_8-Cu and **(b)** NiPc-O_8-Cu MOF after 30 min exposure to 80, 40, 20, and 10 ppm of CO. **(c)** Responses ($-\Delta G/G_0$) of CoPc-O_8-Cu MOF and NiPc-O_8-Cu after 30 min exposure versus concentration of CO. Error bars represent standard deviation from the average response based on at least three devices.

Author Manuscript Author Manuscript Author Manuscript Author Manuscript

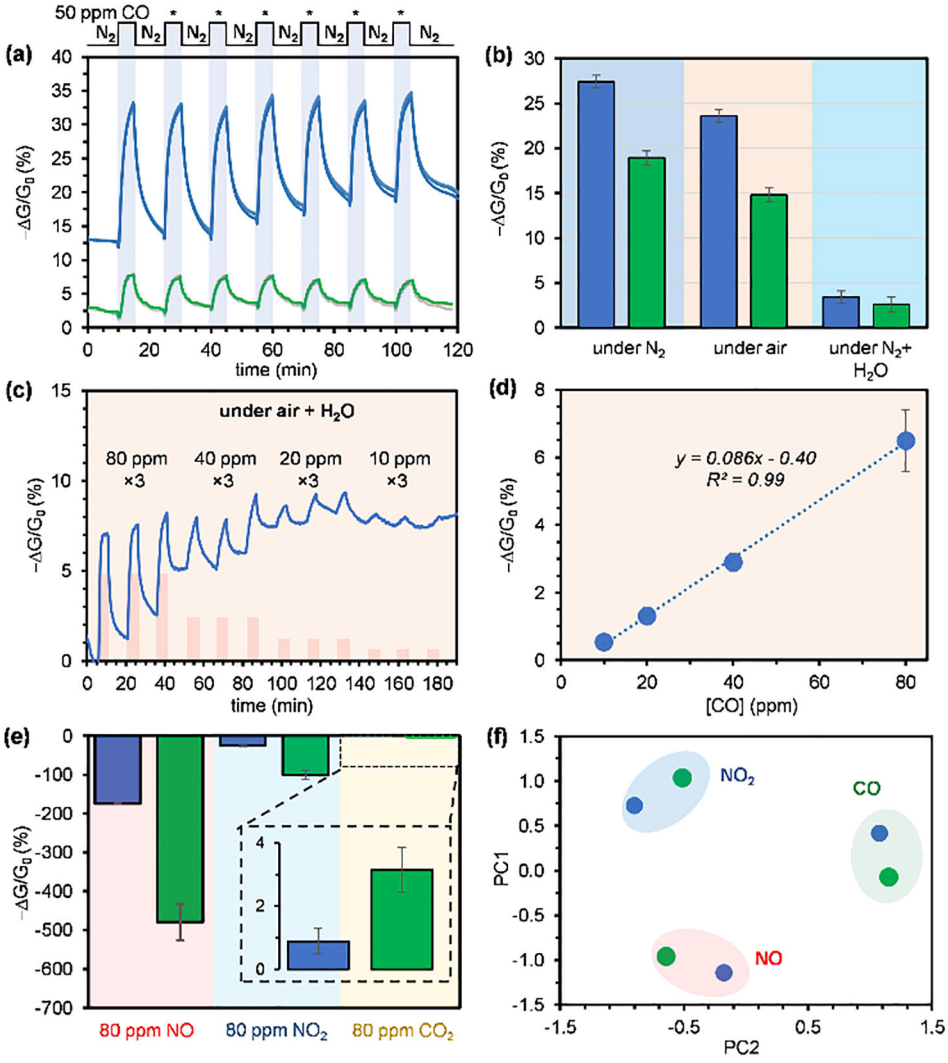

Figure 3.

(a) Sensing traces of 7 sequential exposure-recovery cycles to 50 ppm CO using CoPc-O_8-Cu (blue) and NiPc-O_8-Cu (green). Each cycle comprised a 5 min exposure and 10 min recovery. (b) Response of CoPc-O_8-Cu (blue) and NiPc-O_8-Cu (green) to 80 ppm CO in N_2, air, and humid N_2 with 5000 ppm of H_2O (18% relative humidity, RH). (c) Sensing traces of CoPc-O_8-Cu to consecutive exposure-recovery cycles of 80, 40, 20, and 10 ppm of CO in the air with 5000 ppm of H_2O. For each cycle, the exposure and recovery time were 5 and 10 min, respectively. For each concentration, three exposure-recovery cycles were performed. (d) Response-concentration relationship of CoPc-O_8-Cu under consecutive CO exposures in humidified air (5000 ppm H_2O, 18% relative humidity, RH). (e) Response of the CoPc-O_8-Cu (blue) and NiPc-O_8-Cu (green) to 80 ppm of NO, NO_2, and CO_2. (f) PCA for NiPc-O_8-Cu (green) and CoPc-O_8-Cu (blue) showing capability for differentiating 80 ppm of NO_2, NO, and CO.

Author Manuscript Author Manuscript Author Manuscript Author Manuscript

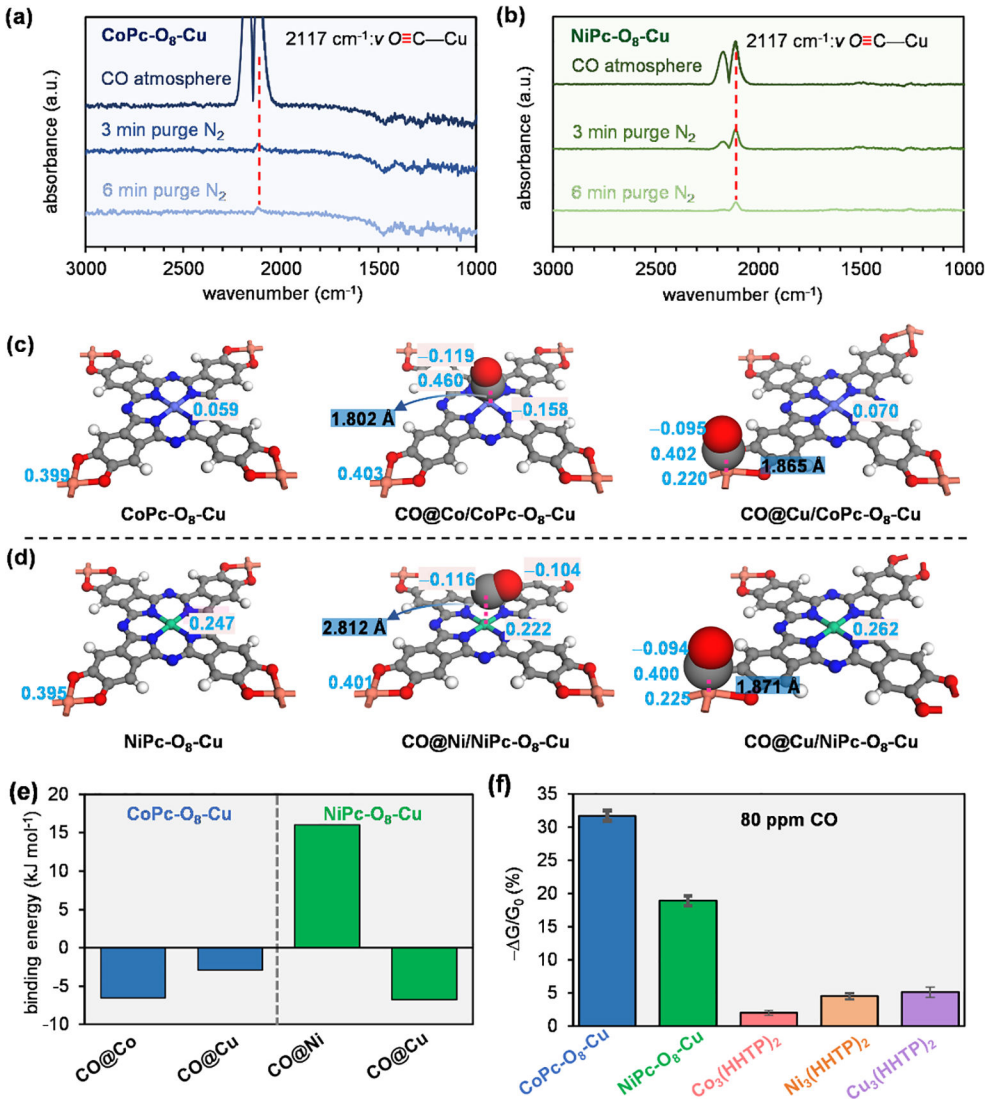

Figure 4.

(a) DRIFTS spectra of CoPc-O_8-Cu and **(b)** NiPc-O_8-Cu after exposure to 1% CO (10000 ppm) of for 6 min. The spectra are presented as double beam experiments with pristine MPc-O_8-Cu MOFs used as the reference. **(c)** The optimized structures of CoPc-O_8-Cu, CO@Co/CoPc-O_8-Cu, CO@Cu/CoPc-O_8-Cu. **(d)** The optimized structures of NiPc-O_8-Cu, CO@Ni/NiPc-O_8-Cu, and CO@Cu/NiPc-O_8-Cu. The calculated values of the Mulliken charge are labeled with blue. The CO•••M lengths are labeled with black. **(e)** Bindning free energies of CO at different sites of the MPc-O_8-Cu MOFs**. (f)** Comparison of the sensing response of MPc-O_8-Cu and $M_3(HHTP)_2$ MOFs to 80 ppm of CO in N_2.